Computational Materials Science 195 (2021) 110499

Contents lists available at ScienceDirect

Computational Materials Science

journal homepage: www.elsevier.com/locate/commatsci

Exploring the different roles of graphene and its derivatives as nano-additives at amorphous carbon surface through reactive molecular dynamics approach

Xiaowei Li [a,b,*], Dekun Zhang [a], Kwang-Ryeol Lee [b,*]

[a] School of Materials and Physics, China University of Mining and Technology, Xuzhou 221116 PR China
[b] Computational Science Center, Korea Institute of Science and Technology, Seoul 136-791, Republic of Korea

ARTICLE INFO

Keywords:
Graphene derivative
Amorphous carbon
Lubricant additive
Reactive molecular dynamics
Friction mechanism

ABSTRACT

Graphene (G) and its derivatives exhibit great potential as oil-based additives to enhance the anti-friction capacity of amorphous carbon (a-C) interface for industrial applications. However, due to the structural diversity of G derivatives and the limitation of experimental characterization, the difference of intrinsic G and its derivatives in improving the lubricity and the underlying tribochemical information is still unclear, leading to a lack of fundamental understanding of the friction mechanism. Here, we address these issues through the atomic-scale simulation and demonstrate that compared to the intrinsic G, its derivatives can further reduce the friction resistance at a-C surface, especially the chair-type graphane with the reduction of friction coefficient by 86%. Most importantly, the fundamental friction mechanism caused by G derivatives mainly attributes to the G-induced cross-linking and cold welding of mated a-C surfaces, although it is also affected by the passivation of the friction interface and the hydrodynamic lubrication of base oil. These outcomes can guide the R&D of advanced a-C/lubricant synergy systems for technical applications.

1. Introduction

Since the discovery of graphene (G) by A. Geim and K. Novoselov [1–3], G and G-like materials have been paid much attention in scientific and engineering fields because of their special 2-dimension (2D) structure and outstanding chemical, mechanical, electronic, optical, and thermodynamic properties [4–10]. Until now, many G-related materials have been synthesized experimentally or designed theoretically, such as hydrogenated graphene [11], graphane [4], oxidized graphene [12], graphyne [13], tetrahexcarbon [14], and so on, which are called G derivatives. They have been widely used as dopant candidates, such as anti-corrosion additive in coating [15,16], conductive additive for lithium-ion battery [17], electrolyte additive [18], anti-shrinkage additive [19], and anti-irradiation additive [20], to endow the materials with enhanced or new properties.

Recently, due to the 2D structure and weak intermolecular interaction between layers, G derivatives as friction modifier additives exhibit the great potential to functionalize the fluid lubricant and thus strengthen the tribological performance of the metal or coated surface [8,21–28]. For example, Zhao *et al.* [8] reported that after adding 0.05 wt% polyethylene glycol-modified G into the water solution, both the wear rate and friction coefficient were reduced by 81.23% and 39.04%, respectively, as compared to the pure water case. Similar behavior was also observed by Kinoshita *et al.* [22] when the G oxide monolayer sheet was introduced into the water as an additive. Liu *et al.* [23] found that compared to the intrinsic G, the system containing fluorinated G as a lubricant additive had 51.4% and 90.0% decrease in friction coefficient and wear rate, respectively, which resulted from the increased interlayer distance. He *et al.* [24,25] clarified that during the friction process, the G structure with regular edge and high exfoliation degree was more conducive to form the continuous, thick, and ordering tribofilm.

However, in practical applications, the synergistic lubrication system, which is composed of G nano-additive, fluid lubricant, and amorphous carbon (a-C) film [29–31], normally arouses widespread research interests [32–35]. It can overcome the friction and wear failure of mechanical components under inevitable oil-poor or oil-free conditions. In such a composite system, the a-C film as an excellent solid lubricant can provide additional protection against friction under instantaneously harsh condition; the fluid lubricant separates the mated surface against cold welding; while for the intrinsic G or its derivative as a lubricant

* Corresponding authors at: School of Materials and Physics, China University of Mining and Technology, Xuzhou 221116 PR China.
E-mail addresses: lixw0826@gmail.com (X. Li), krlee@kist.re.kr (K.-R. Lee).

https://doi.org/10.1016/j.commatsci.2021.110499
Received 18 October 2020; Received in revised form 2 April 2021; Accepted 5 April 2021
Available online 19 April 2021

additive, it plays critical role in weakening the rupture of liquid lubricant and also enhancing the anti-friction capacity in synergism with lubricant and a-C film [26–28,32]. For example, Wang *et al.* [26–28] demonstrated that at the a-C-coated surface, the G additive could stack to form a thick tribofilm under high applied load, which effectively separated the two contact surfaces against friction.

Although in our previous study [32] we have conveyed the advantage of G as an oil-based additive in effectively improving the friction behavior when compared with the nanotube and fullerene additives, the tribochemical information underlying the transformation of the a-C/oil/G-composited interface is still not fully understood. This is due to its strong dependence on the structure of intrinsic G and its derivatives (size, layer, content, functionalized group) [8,22–25] and the limitation of experimental characterization. Even less is known about the difference of intrinsic G and its derivatives in the improvement of lubricity from the atomic scale, leading to the lack of fundamental understanding of friction mechanism and also limiting the development of effective lubrication system without numerous heuristic experiments. So in this work, we fabricated the a-C/lubricant model and systematically demonstrated the friction dependence of intrinsic G and its derivatives as nano-additives through the reactive molecular dynamics (RMD) approach. An in-depth analysis of the structural evolution with G derivatives at the friction interface was conducted to explore the underlying friction mechanism by comparing to that with the intrinsic G, which has not been reported theoretically and experimentally before. These can guide the selection and design of G-based lubricant additive and accelerate the development of the high-efficient a-C/lubricant synergy system for applications. The simulation models and parameters were given in Section 2; the change of friction results with G additives, including friction coefficient, width and structural evolution of friction interface, stress of H atoms from G and base oil molecules, interaction between a-C and G additive, and diffusion behavior of base oil were determined in Section 3, which was followed by the discussion of the friction mechanism.

2. Computational details

All simulations were performed by Large-scale Atomic/Molecular Massively Parallel Simulator code [36]. Similar to our previous study [32], the a-C/lubricant/a-C friction model was fabricated, as shown in Fig. 1a. It consisted of upper a-C as counterface, fluid lubricant, and lower a-C as substrate, Among them, the a-C model (size: 42.88 × 40.36 × 31.00 Å^3) was obtained using atom-by-atom deposition [37], which contained 6877 carbon atoms; the sp^3 fraction, sp^2 fraction, and density at the stable growth region of a-C model were 24 at.%, 72 at.%, and 2.7 g/cm^3, respectively. Fluid lubricant contained the linear alpha olefin, C_8H_{16}, as representative base oil [38] and the G fragment as lubricant additive, in which 45 repeated units for C_8H_{16} molecule were used for each case, while the G fragment (Fig. 1b) was composed of 66 C atoms and its structure ranged from intrinsic G to hydrogenated graphene, graphane (chair-type, boat-type) [4], oxidized graphene (–O, –OH, and –O/–OH) [4], graphyne [4], hydrogenated graphyne [4], and tetrahexcarbon [14]. Previous study [32] have confirmed that compared to the G-free case, using such dimension of graphene-related material as additive (Fig. 1) could obviously reduce the friction coefficient.

Before the friction simulation, a three-layer assumption was adopted in each friction system (Fig. 1a): (i) the rigid layer to imitate the semi-infinite system; (ii) the thermostatic layer kept at a constant temperature of 300 K using NVE ensemble with Berendsen thermostat [39] to avoid overheating of the system; (iii) the free layer to simulate the

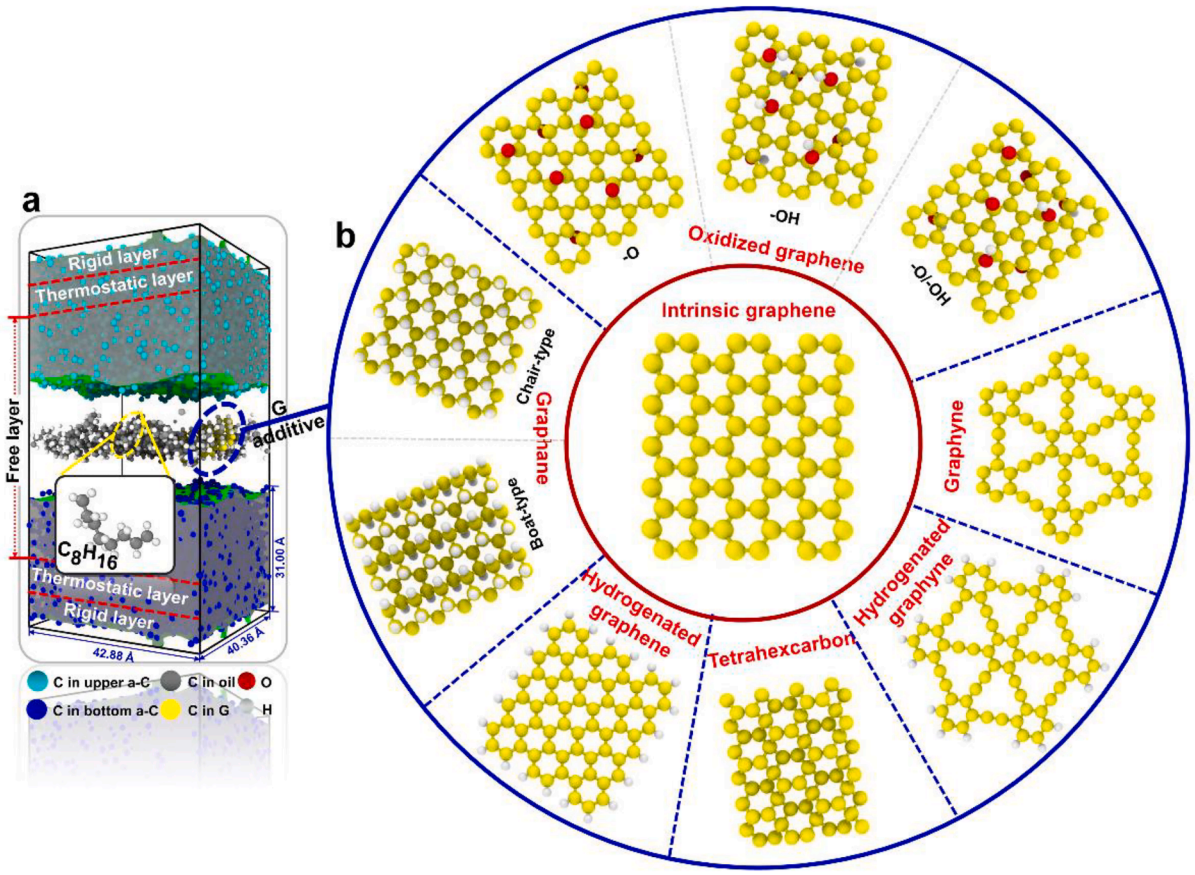

Fig. 1. Friction model and G fragments used as lubricant additives in this work. (a) Friction model composed of a-C, C_8H_{16} as base oil, and G fragment as lubricant additive. (b) G fragments including intrinsic G and its derivatives.

friction-induced structural evolution. During the friction process, the geometric optimization of system was taken first at 300 K for 2.5 ps; then, the rigid layer of upper a-C in Fig. 1a was loaded to the constant contact pressure (5 GPa) during 25 ps; after that, the rigid layer of upper a-C moved along the *x* direction for 1250 ps in the sliding velocity of 10 m/s and fixed contact pressure (5 GPa). Although these values of contact pressure and sliding velocity were higher than experimental ones, our and other previous works [32,35,40–43] have confirmed that they were appropriate for sufficiently sampling the phase space and examining the friction behavior and tribochemical reactions of a-C film on an atomic scale. After the friction process, the friction coefficient (μ) was calculated according to the friction force and normal force values at the stable friction stage.

Besides, the periodic boundary condition was applied along the *x*- and *y*-directions; the time step of 0.25 fs was used. Reactive force field developed by Tavazza et al. [44] was used to evaluate the interactions between a-C, base oil, and G derivatives, which has been fully validated suitable for our simulated systems [32,38,40,41]. The cut-off radius values were 1.85 Å for C–C, 1.20 Å for C–H, 0.85 Å for H–H, 1.63 Å for C–O, 1.20 Å for H–O, and 1.50 Å for O–O, respectively [45]. OVITO [46] was used to visualize each friction system. More Information about the model, simulation process and parameters could be found in our previous works [32,38,40,41,47].

3. Results and discussion

3.1. Friction results under intrinsic G and its derivatives as lubricant additives

The changes of friction force and normal force with sliding time are plotted first for each system. Taking the system with chair-type graphane as lubricant additive for example (Fig. 2a), it shows that the system could reach the steady-state friction stage quickly without distinct running-in process, but the changes of friction and normal forces with sliding time still exhibit relatively large fluctuations, which is due to the presence of stick–slip interactions at the interface. This is also observed for other cases. In particular, compared to the lubricant-free case [40], the addition of fluid lubricant could significantly separate the mated a-C surface against the presence of cold welding (insets in Fig. 2a), but the corresponding evolution of interfacial structure strongly depends on the lubricant additives, as will be discussed later. In order to compute the friction coefficient, the friction force and normal force values located at the last 250 ps of the stable friction stage (Fig. 2a) are averaged. Fig. 2b shows the calculated friction coefficients with G or G derivatives, exhibiting strong dependence on the lubricant additives. When the lubricant additive is intrinsic G, the friction coefficient is 1.05. However, the friction coefficient can be tailored at different levels due to the use of the G derivatives instead of intrinsic G. Especially in the system with chair-type graphane as lubricant additive, the friction coefficient is only 0.15, which is reduced by 86% compared to the intrinsic case.

3.2. Determination of friction interface during the sliding process

Under the solid–liquid composite lubrication, especially the boundary lubrication condition, the friction behavior is closely sensitive to the hydrodynamic lubrication of fluid lubricant and the structural evolution of the friction system. In particular, the structure of friction interface, such as the interfacial passivation and the formation of tribolayer, seriously affects the friction property of a-C film, which has been confirmed by previous simulations [35,41,47] and experimental studies [26,33,48]. However, the in-situ characterization of the interfacial structure is not accessible in the experiment, while it can be easily achieved by the simulation approach. Before evaluating the structural evolution of the friction interface, its width should be accurately identified first. Fig. 3 gives the mapping distributions of the number of C and H atoms along with the film depth and sliding time, which are from a-C, G additive, and C_8H_{16} base oil, respectively, in the system with chair-type graphane as additive. For all systems, the interfacial widths are determined, which change in the range of 15.0–12.0 Å with the G derivative. In addition, the different width values of friction interfaces implies the difference in tribo-induced structural transformation and interactions between a-C, G derivative, and base oil molecules at the

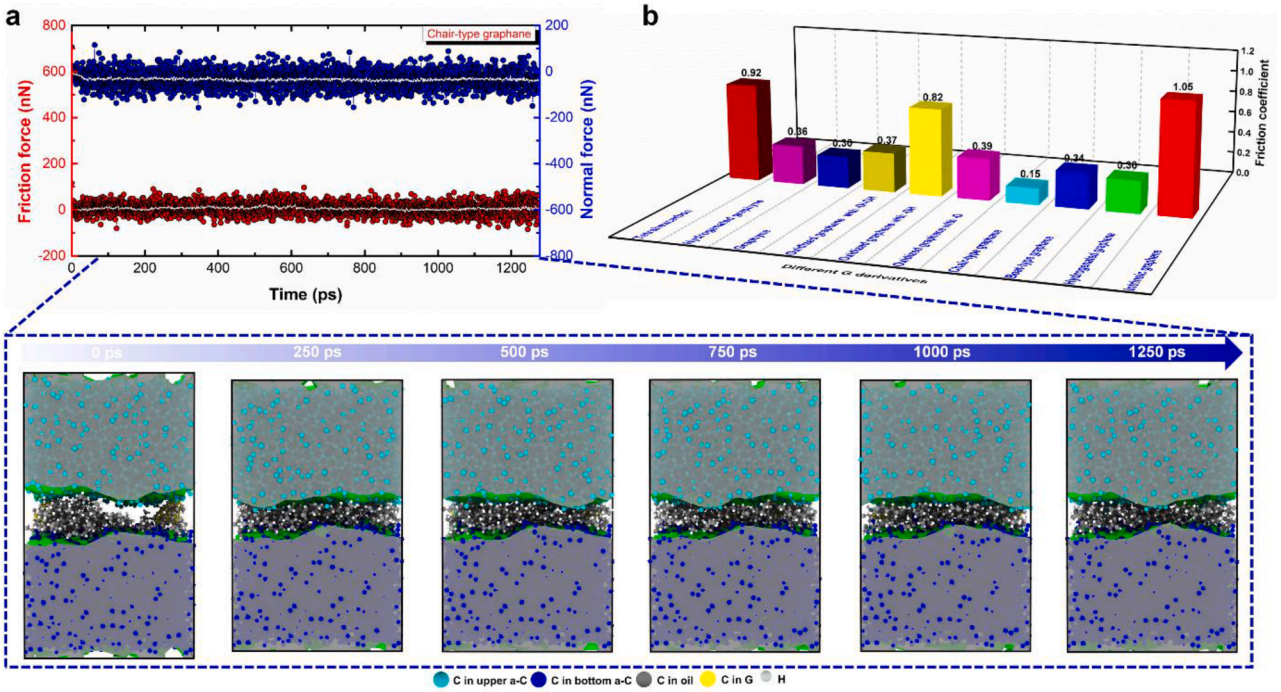

Fig. 2. Friction results under intrinsic G or its derivatives as lubricant additives. (a) Changes of friction force and normal force values with sliding time for the system with chair-type graphane as a lubricant additive, in which the white lines are the smoothed values for each case and the snapshots are the morphologies obtained at different sliding times. (b) Friction coefficients of a-C/lubricant systems with intrinsic G or G derivatives as lubricant additives.

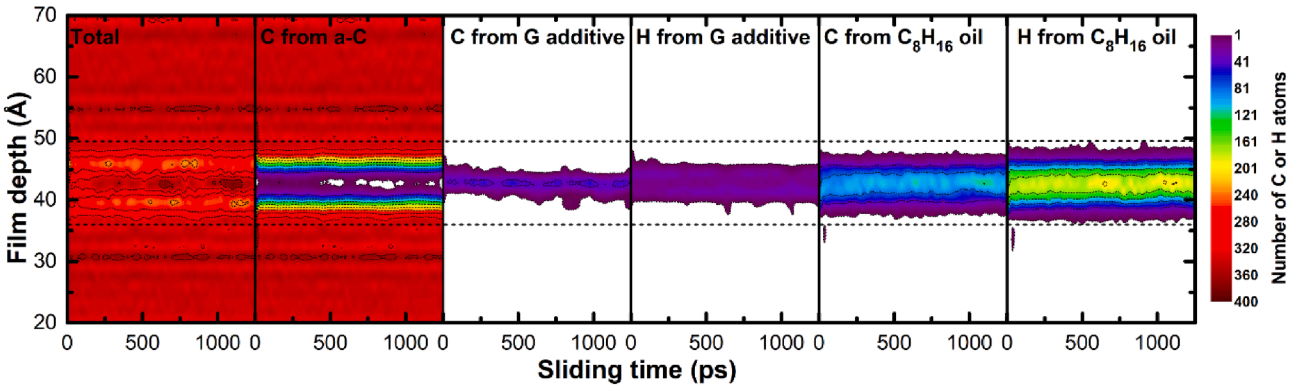

Fig. 3. Mapping distributions of the number of C and H atoms from a-C, G additive, and C_8H_{16} base oil, respectively, in the system with chair-type graphane as lubricant additive during the sliding process.

interface.

3.3. Evolution of interfacial structure during the sliding process

Due to the relatively low normal force [41], C_8H_{16} oil interacts with the mated a-C surfaces, intrinsic G, or its derivatives through intermolecular interaction instead of chemical bonding. There is almost no dissociation of C_8H_{16} molecules occurred. However, the covalent bonds are observed between a-C and intrinsic G or its derivatives, as shown in Fig. 4, being consistent with the previous study [32]. Most importantly, it can be seen that compared to the intrinsic G, the G derivatives exhibit different structural transformations and bonding states with mated a-C surfaces during the sliding processes (Fig. 4). This could not only result in the rehybridization of friction interface to affect the fractions of dangling bonds, but also aggravate the cross-linking of a-C substrate with counterface and thus raise the friction resistance.

The evolution of the C hybridization structure of friction interface for each system is depicted in Fig. 5, which is contributed by the a-C and intrinsic G or its derivatives only. Note that although the intrinsic G or its derivatives show different existing states during the friction processes, such as the step-by-step rupture of intrinsic G and the almost intact structure of hydrogenated graphene (Fig. 4), the friction-induced transformation of interfacial hybridization structure with sliding time is similar for each system. With increasing the sliding time to 1250 from 0 ps, the fractions of 4- and 3-coordinated C atoms at the friction interface increase first and then become stable, which are contrary to the 1- and 2-coordinated C atoms (Fig. 5). This originates from the change of interfacial stress according to the *P-T* phase diagram [38,41,49]. Due to the very low fraction of 1-coordinated C atoms at the interface and its slight difference between all systems, its effect on the friction behavior can be ignored. However, the un-passivated atoms, including the 3- and 2-coordinated C atoms could exert strong intermolecular interaction on the base oils. Their quantitative values after the sliding time of 1250 ps are calculated to comparatively analyze the contribution of un-passivated C atoms to the friction behaviors of systems under different G derivatives, as will be discussed later. However, it should be noted that the difference in interfacial hybridization structure (Fig. 5) is closely

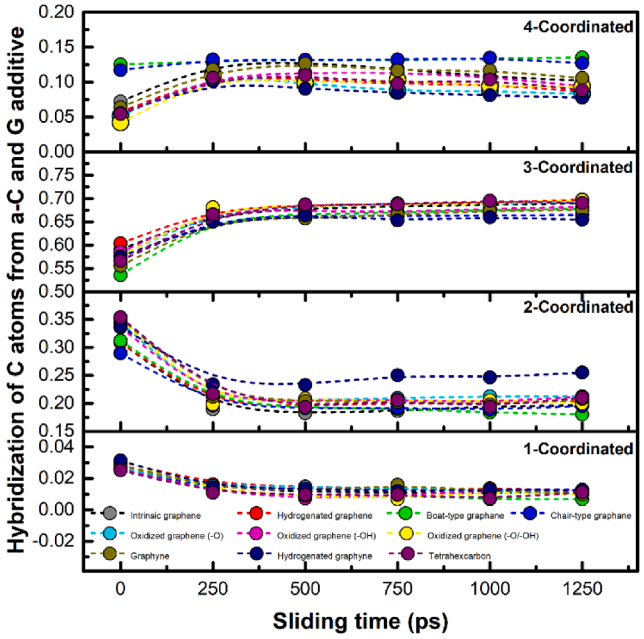

Fig. 5. Change of hybridized structure of friction interface with sliding time, which is contributed by a-C and G additive only.

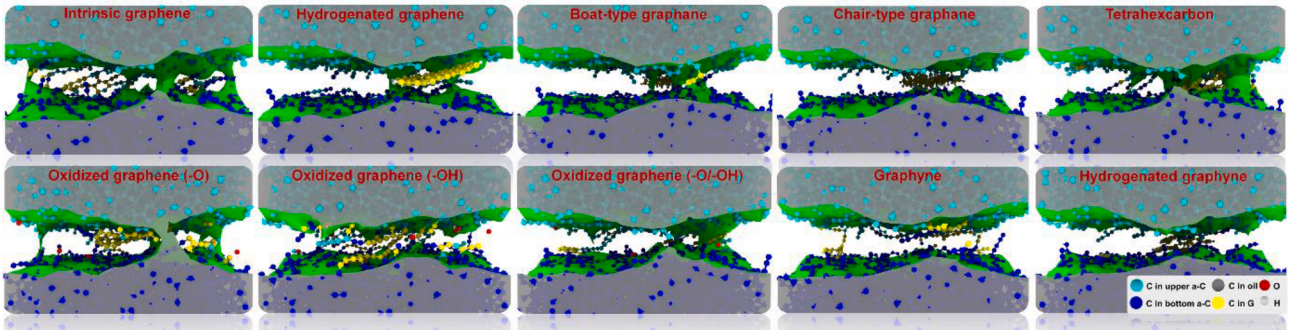

Fig. 4. Interfacial snapshots of all friction systems after sliding time of 1250 ps, in which the C_8H_{16} oil molecules are neglected for view. The surface mesh caused by C atoms in a-C is marked as green color.

affected by the original structure and dissociation of G additive, the bonding of G additive with a-C surfaces, the bonding between mated a-C films, and the stress evolution of H atoms. In particular, previous studies [47,50] revealed that the tensile stress state of H in oil molecules could promote the self-passivation of contacted a-C surfaces to improve the mobility of base oil molecules.

3.4. Distribution of the stress of H atoms from oil molecules

Fig. 6 and Fig. S1 of Supplementary Data show the stress distributions of H atoms from C_8H_{16} base oil molecules during the sliding process for each case. It is observed that for the system with intrinsic G as a lubricant additive (Fig. 6a), the H atoms in C_8H_{16} oils give the tensile stress state. Besides, the stress mainly distributes at the center of the friction interface, which is almost unchanged with sliding time. However, when the intrinsic G is substituted by chair-type graphane (Fig. 6b) and other G derivatives (Fig. S1 of Supplementary Data), this has slight effect on the stress state (tensile stress) and value of H atoms in the C_8H_{16} base oil, suggesting that the H stress in base oil exhibits similar effect on the passivation of the interfacial structure under different G additives. Hence, the difference in hybridization structure of friction interface in Fig. 5 is mainly dominated by the interaction between a-C and a-C or G additive.

3.5. Interaction between a-C and intrinsic G or its derivatives

Fig. 7a shows the distribution of bond numbers between intrinsic G and a-C at the friction interface, which can be used to describe their bonding interaction. Fig. 8a gives the corresponding structural snapshots of friction interface and intrinsic G during the sliding process. Note that with increasing the sliding time to 1250 from 0 ps, the side atoms of intrinsic G tend to covalently bond with two mated a-C surfaces. Under the friction-induced shearing effect, this initial G structure is seriously ruptured step-by-step following the high tensile stress of C atoms in intrinsic G (Fig. 7b), which contributes to the fraction of 2-coordinated C atoms at the interface (Fig. 5). Although the G-induced cross-linking can serve as a supporting site against the applied normal load, which is favorable for the mobility of base oil molecules, the dissociation of intrinsic G structure also increases the roughness of the a-C surface significantly. Hence, the friction interface cannot be wetted by C_8H_{16} oils uniformly, resulting in the presence of serious cold welding, as confirmed by Fig. 7c.

Compared to the case with intrinsic G, the similar interaction of G with a-C and the corresponding rupture of G structure are also observed for the oxidized graphene (–O, –OH, and –O/–OH), graphyne, and tetrahexcarbon, respectively (Figs. S2–S6 of Supplementary Data). However, in the system with oxidized graphene (−O) or oxidized graphene (–O/–OH), there are still small G fragments remained. Especially for three oxidized structures (Figs. S2–S4 of Supplementary Data), the C-O bonds are preferentially dissociated and the generated -O or –OH groups bond with a-C, thus leading to the fast reduction of 2-coordinated C atoms at the interface during the short running-in process (Fig. 5). This is consistent with Moseler's report [35]. Moreover, for the system with graphyne (Fig. 4 and Fig. S5 of Supplementary Data), most of C atoms dissociated from graphyne passivate the a-C surface rather than cross-link with mated a-C surfaces and thus there is no obvious increase of

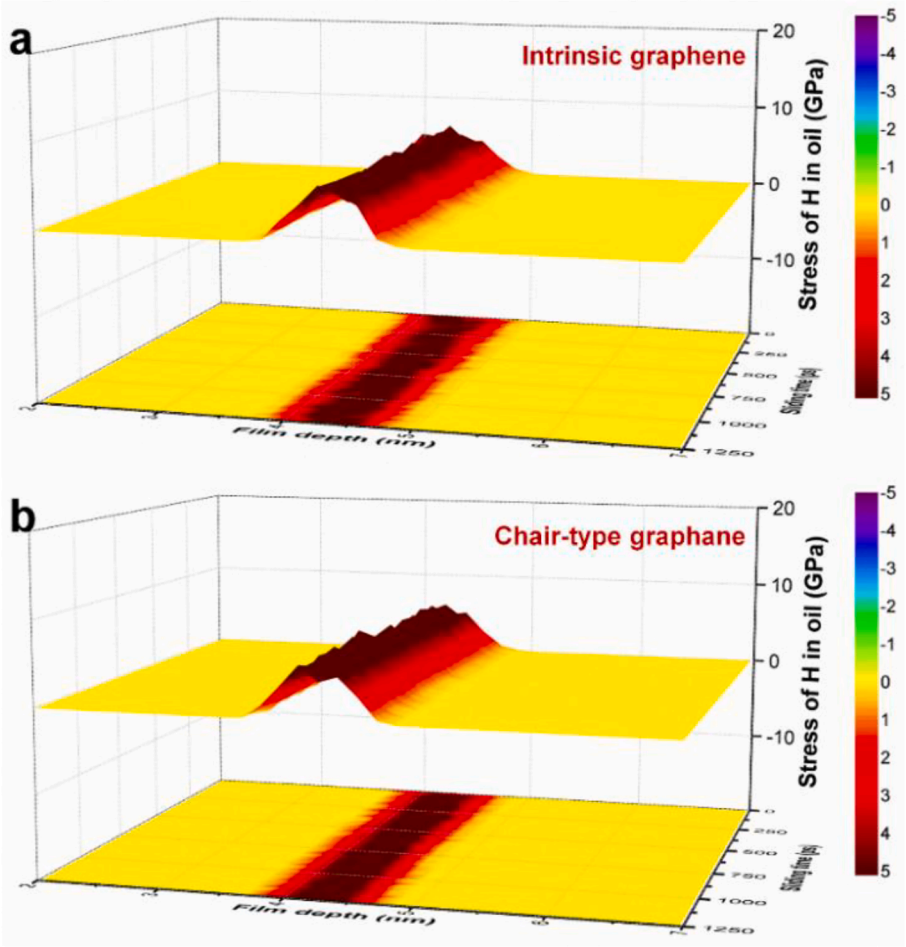

Fig. 6. Distribution of the stress of H atoms from C_8H_{16} oil molecules for the systems with (a) intrinsic G and (b) chair-type graphane as lubricant additives, respectively.

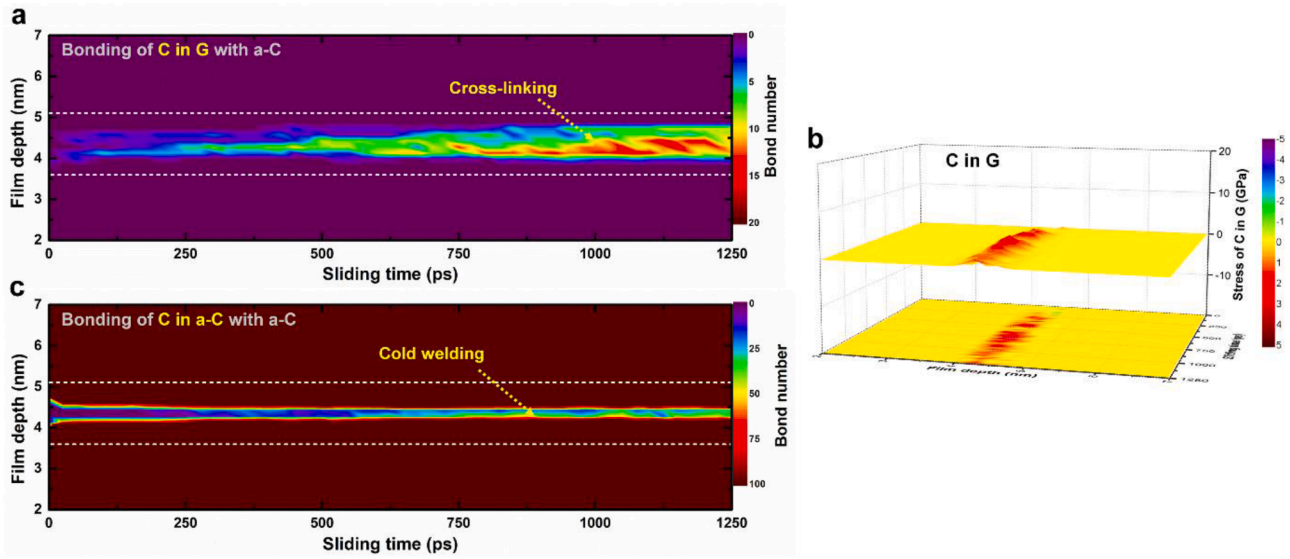

Fig. 7. Interaction of a-C with intrinsic G additive or a-C during the friction process. (a) Distribution of bond numbers between intrinsic G and a-C at the friction interface. (b) Stress distribution of C atoms in intrinsic G. (c) Distribution of bond numbers between mated a-C surfaces at the friction interface.

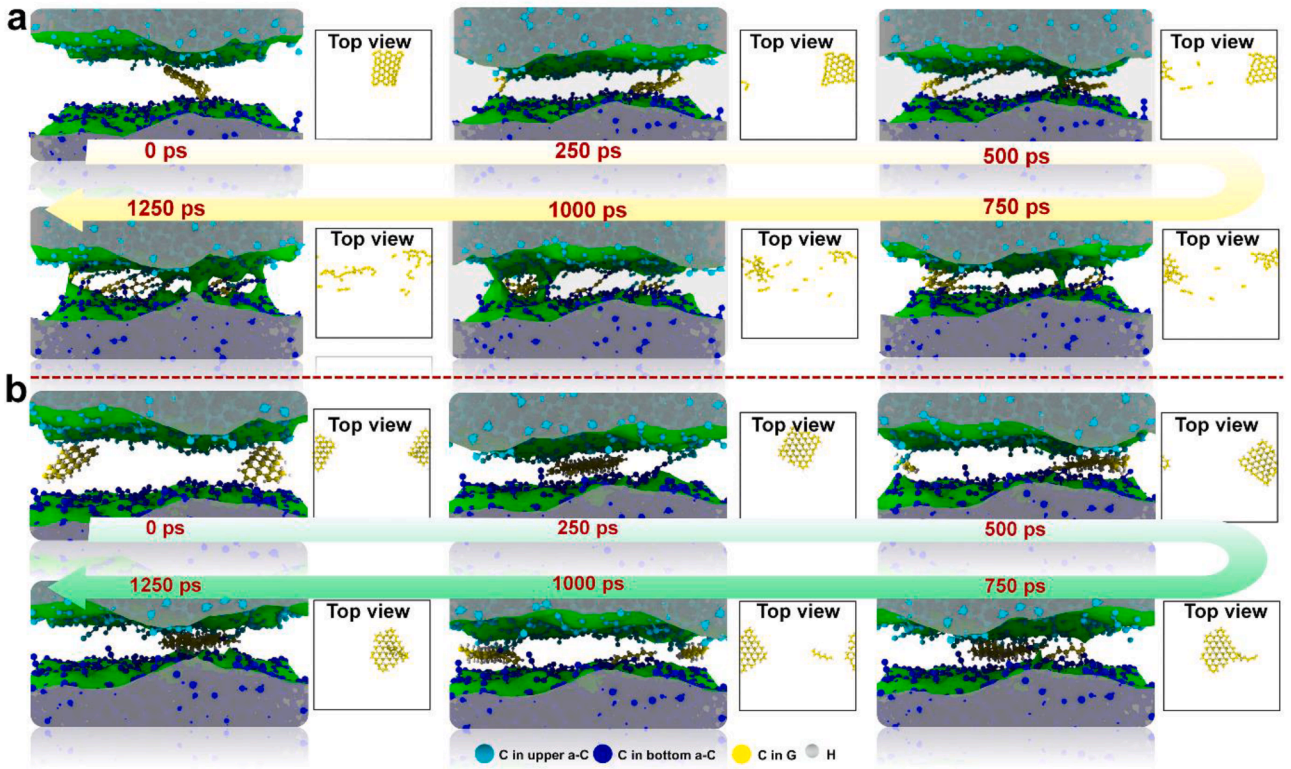

Fig. 8. Corresponding structural evolutions of the interface and (a) intrinsic G or chair-type graphane during the sliding processes, in which the base oil molecules are neglected.

interfacial roughness, accounting for the weak cold welding between mated a-C surfaces.

Moreover, for the systems with hydrogenated graphene, boat-type graphane, chair-type graphane, or hydrogenated graphyne, the addition of H can suppress the activity of side atoms of G structure significantly against cross-linking, so these initial G structures are almost preserved after the sliding processes, as illustrated in Fig. 8b, Fig. 9a, and Figs. S7–S9 of Supplementary Data, respectively. However, they also exhibit different bonding interactions between a-C and G: anchoring to one a-C surface for hydrogenated graphene (Fig. S7 of Supplementary Data) and chair-type graphane (Fig. 9a), free-standing for boat-type graphane (Fig. S8 of Supplementary Data), and transformation from anchoring to cross-linking for hydrogenated graphyne (Fig. S9 of Supplementary Data), respectively, which induce the different friction behaviors. Besides, the C atoms in these four G derivatives show the compressive stress state, while the H atoms give the tensile stress state (Fig. 9b and Figs. S7–S9 of Supplementary Data).

In particular, due to the high H content in the boat-type graphane

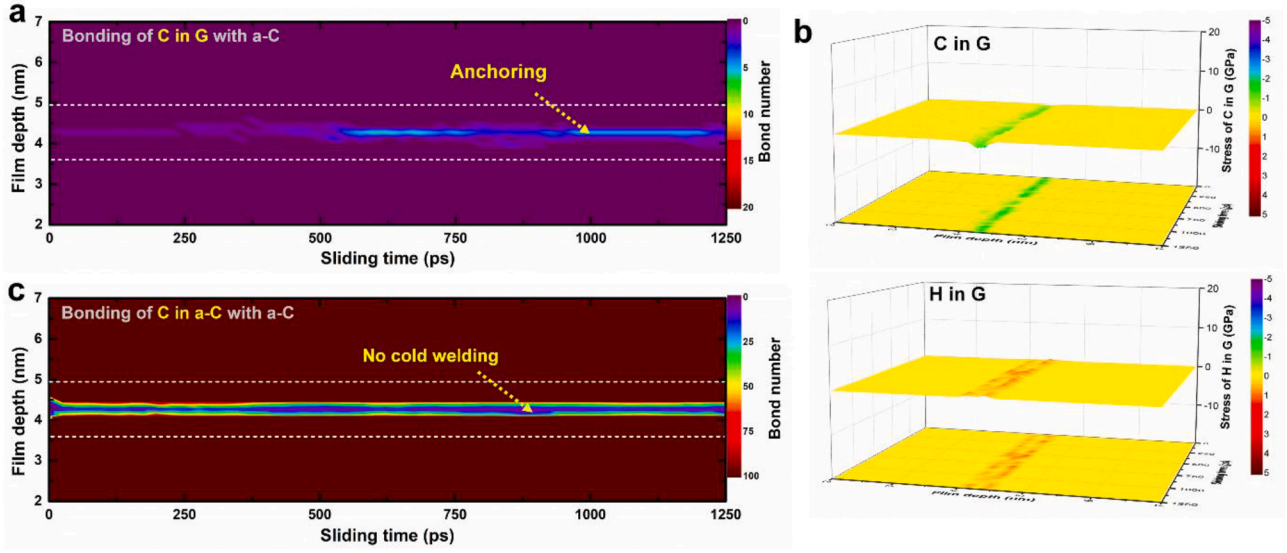

Fig. 9. Interaction of a-C with chair-type graphane additive or a-C during the friction process. (a) Distribution of bond numbers between chair-type graphane and a-C at the friction interface. (b) Stress distribution of C and H atoms in chair-type graphane. (c) Distribution of bond numbers between mated a-C surfaces at the friction interface.

and chair-type graphane, high tensile stress of H atoms (Fig. 9b and Fig. S8c of Supplementary Data) leads to the low 2-coordinated C fraction at the friction interface [47], as illustrated in Fig. 5. Furthermore, for the graphane with the chair-type distribution of H atoms, this can weaken the mutual interference among H atoms in the G structure. So on the one hand, the stronger repulsive force is obtained as compared to the boat-type structure. On the other hand, it is favorable to the regular stress distribution of H atoms at the two lateral sides of C atoms. The strong repulsive force between H atoms from both the G structure and C_8H_{16} molecules can effectively prohibit the two mated a-C surfaces from cold welding (Fig. 9c).

3.6. Diffusion behavior of C_8H_{16} base oil

Except for the interfacial structure, the contribution from the hydrodynamic lubrication of used base oil molecules also plays a critical role in the friction behavior of the a-C/lubricant system. In order to reveal the effect of the mobility of base oil on the friction behavior, the mean square displacement (MSD) is estimated for each system [38,41].

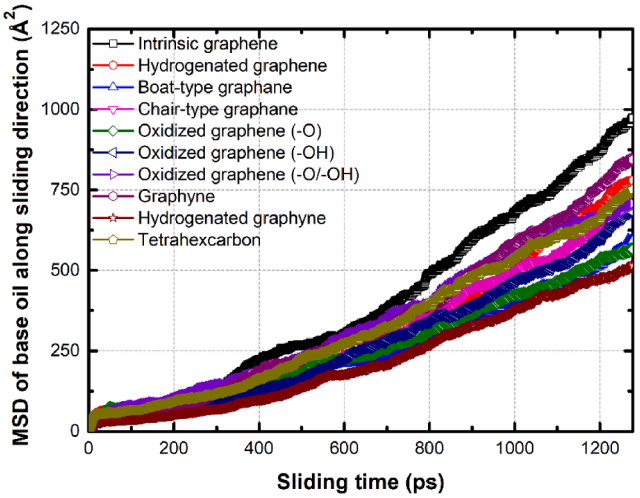

Fig. 10. MSD curve for C_8H_{16} base oil molecules in each system during the friction process.

It is an effective approach to quantify the diffusion of C_8H_{16} oil along the sliding direction. Fig. 10 shows the MSD curve for C_8H_{16} base oil molecules in each system during the friction process, which increases gradually with sliding time.

As well know that the mobility of C_8H_{16} base oil lubricant can be affected by the structural properties (viscosity, chain length, *et al.*) and content of base oil [38,51], temperature [52,53], and structure of friction interface [41]. First, in the present work, the same structure and content of base oil are used for each case. In addition, the flash temperature between both surface asperities is estimated (Fig. S10 of Supplementary Data), which is kept at about 304 K for each system because of the small contact pressure [38]. Therefore, the mobility of C_8H_{16} base oil molecules should be mainly dominated by the complicated structure of friction interface, including the fraction of dangling bonds at a-C surface, cross-linking of mated a-C surfaces, and surface roughness.

For the system with intrinsic G, it shows the highest MSD value of C_8H_{16} molecules compared to other cases, attributing to the direct and indirect cross-linking of mated a-C surfaces which take over most of the applied load. This can be confirmed by the lowest value of the real contact area (451 $Å^2$ only). This is similar to the cases with graphyne or oxidized graphene (–OH), respectively. Although the passivation of a-C surface caused by dissociated G fragments and the smoothing of a-C surface caused by the anchoring of G structure (or G fragments) are favorable to the shearing motion of friction interface, they also increase the normal load exerted on C_8H_{16} molecules and thus weaken the diffusion of oil molecules along the sliding direction, such as oxidized graphene (–O, –O/–OH), chair-type graphane, boat-type graphane, and hydrogenated graphene. But for the hydrogenated graphyne, the high fraction of dangling bonds (Fig. 5) causes the slowest increase of MSD value with sliding time. It should be mentioned that for most cases, the mobility of C_8H_{16} lubricant is affected by the abovementioned factors in synergism. It is hard to give an accurate explanation for the different MSD values of C_8H_{16} lubricant between these friction systems. Further calculations are required, but it will be discussed elsewhere and the present work mainly focuses on the friction mechanism induced by different G derivatives.

3.7. Friction mechanism

As we all know that the friction, especially the a-C/liquid composite lubrication, is a very complicated process, which is closely sensitive to

the Hertzian contact pressure [41], sliding velocity [54], temperature [52,53], structure of mated a-C film [55,56], evolution of interfacial structure to form the graphitized transfer layer [8,26,28] or to passivate the surface dangling bonds [38,41], structural properties of fluid lubricant (mobility, viscosity, chain length, *et al.*) [38,57], and interaction of a-C with lubricant [35]. Due to the limitation of experimental characterization in-situ, most of the factors, especially the structural evolution of friction interface, cannot be accurately evaluated in experiment, while they can be undertaken by the RMD simulation approach.

For each system simulated in this study, the same a-C film is used. The friction parameters, including contact pressure and sliding velocity, remain at 5 GPa and 10 m/s, respectively. The rise of flash temperature at the friction interface is also same (304 K). Therefore, in order to shed light on the difference in friction mechanism induced by intrinsic G and its derivatives, the fractions of both 3-coordinated and 2-coordinated C atoms at the friction interface, bond number between intrinsic G or its derivatives and a-C, and bond number between mated a-C surfaces after the friction time of 1250 ps are counted (see Table S1 of Supplementary Data). Besides, the MSD values of C_8H_{16} oil (last 200 ps in Fig. 10) are also fitted to obtain the diffusion coefficient (Table S1 of Supplementary Data) in each system according to the following equation [58]:

$$MSD = 6Dt \tag{1}$$

where D is the diffusion coefficient; t is the diffusion time. Moreover, the shearing strength in Table S1 of Supplementary Data is also calculated for each case as follows [41]:

$$\mu = \frac{S}{\sigma} \tag{2}$$

where σ is the Hertzian contact pressure (GPa) which is 5 GPa in the present work; μ is the friction coefficient; S is the shearing strength (GPa).

Fig. 11 plots the relationship of shearing strength with the 3-coordinated C fraction, the 2-coordinated C fraction, the bond number between intrinsic G or its derivatives and a-C, the bond number between mated a-C surfaces, and the diffusion coefficient for C_8H_{16} oil, which can be described as follows:

$$S = \mathrm{m} \times \frac{B_{a-C/G} \cdot B_{a-C/a-C} \cdot B_1 \cdot B_2}{D} \tag{3}$$

where m is a constant value, D is the diffusion coefficient for C_8H_{16} oil, B_1 is the 2-coordinated C fraction at the interface, and B_2 is the 3-coordinated C fraction at the interface; $B_{a\text{-}C/G}$ is the bond number between a-C and intrinsic G or its derivatives, which is contributed via the anchoring or cross-linking of G with a-C and the re-bonding of a-C with dissociated G fragments; $B_{a\text{-}C/a\text{-}C}$ represents the bond number between mated a-C surfaces, corresponding to the cold welding. It can be seen that when the intrinsic G is introduced into base oil as a lubricant additive, there is a high bond number between a-C and G because of the dissociation and re-bonding of G with mated a-C surfaces, which causes the presence of strong cross-linking (Fig. 7a, Fig. 8a, and Fig. 11). Although it shows the maximal diffusion coefficient of C_8H_{16} oil (Fig. 11), this strong cross-linking prohibits the sliding of friction interface (see Supplementary Movie 1) and thus results in the high shearing strength following the high friction coefficient (Fig. 2b). The high friction coefficient is also contributed by the cold welding between mated a-C surfaces (Fig. 11).

Compared to the intrinsic G, hydrogenating the G structure (such as hydrogenated graphene, boat-type graphane, and chair-type graphane) reduces the number of active C atoms. These G derivatives can anchor to one a-C to smooth the friction interface, which effectively suppresses the occurrence of G-induced cross-linking (Fig. 9a, and Fig. 11) and the dissociation of G structure (Fig. 8b and Figs. S7–S8 of Supplementary Data). Hence, the shearing strength (Fig. 11) is reduced obviously following the low friction coefficient (Fig. 2b, see Supplementary Movie 2). In particular, when the chair-type graphane is selected as lubricant additive, the shearing strength is decreased by 86% as compared to the case with intrinsic G. It mainly attributes to the drops of G-induced cross-linking and cold welding between mated a-C surfaces. Besides, it is also caused by the high repulsive force of H atoms in hydrogenated G structure and C_8H_{16} base oil (Fig. 11 and Fig. 9b), decreasing the fraction of interfacial dangling bonds, as confirmed by previous reports [47,50].

For the OH-functionalized G or tetrahexcarbon as lubricant additive, they also show the high friction coefficients, close to the case with intrinsic G, which is also due to the existence of serious cold welding and G-induced cross-linking between mated a-C surfaces (Fig. 11, see Supplementary Movie 3). However, when the –OH groups inG structure are fully or partially replaced by -O, the friction coefficient can be reduced obviously (Fig. 2b), as confirmed by the drop of shearing strength. This change originates from the significantly decreased cross-linking of a-C with both G and mated a-C surface (Fig. 11). In addition, partial G structure, which is still remained during the friction process (Figs. S2 and S4 of Supplementary Data), also smooths the friction interface (Fig. 4), promoting the sliding of mated a-C surfaces (see Supplementary Movie 4). Moreover, for the graphyne as additive, the G-induced cross-

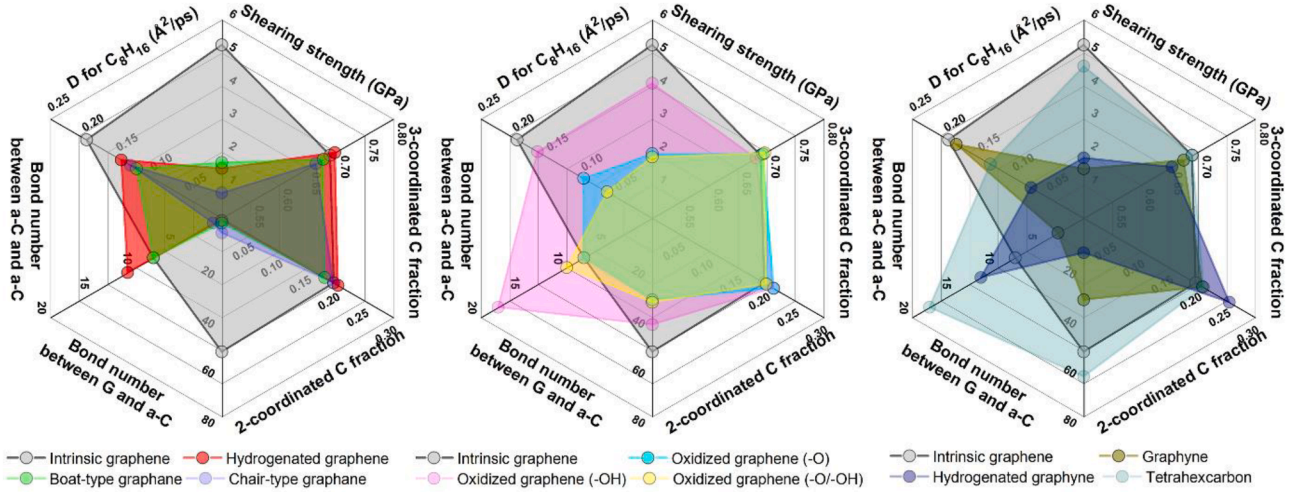

Fig. 11. Relationship between shearing strength and five potential factors including fraction of 3-coordinated C atoms at the interface, fraction of 2-coordinated C atoms at the interface, bond number between intrinsic G or its derivatives and a-C, bond number between mated a-C surfaces, and diffusion coefficient for C_8H_{16} base oil, after the friction processes.

linking and cold welding are weakened significantly (Fig. 11, see Supplementary Movie 5). Combined with the high mobility of C_8H_{16} molecules, it can account for the low friction coefficient. But when the graphyne is hydrogenated as lubricant additive, there is a slight increase of friction coefficient compared to the graphyne case (Fig. 2b), which is related to the increase of 2-coordinated C fraction at the interface and the aggravated cold welding (Fig. 11).

4. Conclusions

In summary, at the atomic scale, we elucidated the friction behavior and corresponding transformation of interfacial structure in the systems of a-C films composited with different fluid lubricants. The evolution of interfacial structure during the sliding process and underlying friction mechanism with G derivatives were discussed with respect to their structures and properties by comparing with the intrinsic G. The results highlighted the critical role of G-based lubricant additive in the formation of an anti-friction interface. Compared to the intrinsic G, G derivatives as oil-based lubricant additive exhibited more potential in reducing the friction coefficient at a-C surface. Especially for chair-type graphane, it resulted in an 86% decrease in friction coefficient. By the systematical analysis of the mobility of base oil and the transformation of interfacial structure, the friction mechanism was unveiled, which mainly depended on the G-induced cross-linking and cold welding between mated a-C surfaces, but it was also contributed by the hydrodynamic lubrication of base oil and the interfacial dangling bonds. It should be mentioned that it is still a big challenge to take the experimental validation for this work due to the limitations of a-C structure, friction parameter, and in-situ characterization of the evolution of interfacial structure. But these findings do disclose the effect of different G derivatives on the friction performance of the a-C interface and the fundamental mechanism to foster the theoretical and experimental works of the lubricant-carbon systems. Most importantly, they can effectively promote the technical selection and design of advanced lubrication systems for engineering applications.

5. Data availability

The authors declare that the data supporting the findings of this study are available within the paper and its Supporting information file.

CRediT authorship contribution statement

Xiaowei Li: Conceptualization, Methodology, Software, Validation, Investigation, Funding acquisition, Conceptualization, Methodology, Software, Validation, Investigation, Writing - original draft, Writing - original draft, Writing - review & editing, Funding acquisition. **Dekun Zhang:** Conceptualization, Funding acquisition, Conceptualization, Writing - review & editing, Funding acquisition. **Kwang-Ryeol Lee:** Conceptualization, Methodology, Resources, Investigation, Supervision, Funding acquisition, Conceptualization, Methodology, Resources, Investigation, Writing - review & editing, Supervision, Funding acquisition.

Declaration of Competing Interest

The authors declare that they have no known competing financial interests or personal relationships that could have appeared to influence the work reported in this paper.

Acknowledgments

This study was supported by the National Natural Science Foundation of China (51772307), Nano Materials Research Program through the Ministry of Science and IT Technology (NRF-2016M3A7B4025402), and the Korea Research Fellowship Program funded by the Ministry of Science and ICT through the National Research Foundation of Korea (2017H1D3A1A01055070).

Appendix A. Supplementary data

Supplementary data to this article can be found online at https://doi.org/10.1016/j.commatsci.2021.110499.

References

[1] K.S. Novoselov, A.K. Geim, S.V. Morozov, D. Jiang, Y. Zhang, S.V. Dubonos, I. V. Grigorieva, A.A. Firsov, Electric field effect in atomically thin carbon films, Science 306 (2004) 666–669.
[2] A.K. Geim, Graphene: status and prospects, Science 324 (2009) 1530–1534.
[3] A.K. Geim, K.S. Novoselov, The rise of graphene, Nat. Mater. 6 (2007) 183–191.
[4] M. Inagaki, F. Kang, Graphene derivatives: graphane, fluorographene, graphene oxide, graphyne and graphdiyne, J. Mater. Chem. A 2 (2014) 13193–13206.
[5] L. Zhang, L. Chen, H. Luo, X. Zhou, Z. Liu, Large-sized few-layer graphene enables an ultrafast and long-life aluminum-ion battery, Adv. Energy Mater. 7 (2017), 1700034.
[6] H. Sun, X. Li, Y. Li, G. Chen, Z. Liu, F.E. Alam, D. Dai, L. Li, L. Tao, J. Xu, Y. Fang, X. Li, P. Zhao, N. Jiang, D. Chen, C.T. Lin, High-quality monolithic graphene films via laterally stitched growth and structural repair of isolated flakes for transparent electronics, Chem. Mater. 29 (2017) 7808–7815.
[7] J. Gong, Z. Liu, J. Yu, D. Dai, W. Dai, S. Du, C. Li, N. Jiang, Z. Zhan, C.T. Lin, Graphene woven fabric-reinforced polyimide films with enhanced and anisotropic thermal conductivity, Compos. Part A 87 (2016) 290–296.
[8] Y. Hu, Y. Wang, Z. Zeng, H. Zhao, X. Ge, K. Wang, L. Wang, Q. Xue, PEGlated graphene as nanoadditive for enhancing the tribological properties of water-based lubricants, Carbon 137 (2018) 41–48.
[9] S. Ren, M. Cui, W. Li, J. Pu, Q. Xue, L. Wang, N-doping of graphene: toward long-term corrosion protection of Cu, J. Mater. Chem. A 6 (2018) 24136–24148.
[10] S. Qiu, W. Li, W. Zheng, H. Zhao, L. Wang, Synergistic effect of polypyrrole-intercalated graphene for enhanced corrosion protection of aqueous coating in 3.5% NaCl solution, ACS Appl. Mater. Interfaces 9 (2017) 34294–34304.
[11] M. Pumera, C.H.A. Wong, Graphane and hydrogenated graphene, Chem. Soc. Rev. 42 (2013) 5987–5995.
[12] C.H. Chen, S. Hu, J.F. Shih, C.Y. Yang, Y.W. Luo, R.H. Jhang, C.M. Chiang, Y. J. Hung, Effective synthesis of highly oxidized graphene oxide that enables wafer-scale nanopatterning: preformed acidic oxidizing medium approach, Sci. Rep. 7 (2017) 3908.
[13] Y. Li, L. Xu, H. Liu, Y. Li, Graphdiyne and graphyne: from theoretical predictions to practical construction, Chem. Soc. Rev. 43 (2014) 2572–2586.
[14] B. Ram, H. Mizuseki, Tetrahexcarbon: a two-dimensional allotrope of carbon, Carbon 137 (2018) 266–273.
[15] C. Chen, S. Qiu, M. Cui, S. Qin, G. Yan, H. Zhao, L. Wang, Q. Xue, Achieving high performance corrosion and wear resistant epoxy coatings via incorporation of noncovalent functionalized graphene, Carbon 114 (2017) 356–366.
[16] J. Zhao, X. Xie, C. Zhang, Effect of the graphene oxide additive on the corrosion resistant of the plasma electrolytic oxidation coating of the AZ31 magnesium alloy, Corros. Sci. 114 (2017) 146–155.
[17] N. Zhu, W. Liu, M. Xue, Z. Xie, D. Zhao, M. Zhang, J. Chen, T. Cao, Graphene as a conductive additive to enhance the high-rate capabilities of electrospun $Li_4Ti_5O_{12}$ for lithium-ion batteries, Electrochim. Acta 55 (2010) 5813–5818.
[18] Z.T. Wondimkun, T.T. Beyene, M.A. Weret, N.A. Sahalie, C.J. Huang, B. Thirumalraj, B.A. Jote, D. Wang, W.N. Su, C.H. Wang, G. Brunklaus, M. Winter, B.J. Hwang, Binder-free ultra-thin graphene oxide as an artificial solid electrolyte interphase for anode-free rechargeable lithium metal batteries, J. Power Sources 450 (2020), 227589.
[19] K. Guo, H. Song, X. Chen, X. Du, L. Zhong, Graphene oxide as an anti-shrinkage additive for resorcinol-formaldehyde composite aerogels, Phys. Chem. Chem. Phys. 16 (2014) 11603–11608.
[20] X. Fan, L. Wang, Graphene with outstanding anti-irradiation capacity as multialkylated cyclopentanes additive toward space application, Sci. Rep. 5 (2015) 12734.
[21] V. Eswaraiah, V. Sankaranarayanan, S. Ramaprabhu, Graphene-based engine oil nanofluids for tribological applications, ACS Appl. Mater. Interfaces 3 (2011) 4221–4227.
[22] H. Kinoshita, Y. Nishina, A.A. Alias, M. Fujii, Tribological properties of monolayer graphene oxide sheets as water-based lubricant additives, Carbon 66 (2014) 720–723.
[23] K. Fan, X. Chen, X. Wang, X. Liu, Y. Liu, W. Lai, X. Liu, Toward excellent tribological performance as oil-based lubricant additive: particular tribological behavior of fluorinated graphene, ACS Appl. Mater. Interfaces 10 (34) (2018) 28828–28838.
[24] J. Mao, J. Zhao, W. Wang, Y. He, J. Luo, Influence of the micromorphology of reduced graphene oxide sheets on lubrication properties as a lubrication additive, Tribo. Int. 119 (2018) 614–621.
[25] J. Zhao, J. Mao, Y. Li, Y. He, J. Luo, Friction-reduced nano-structural evolution of graphene as a lubrication additive, Appl. Surf. Sci. 434 (2018) 21–27.
[26] L. Zhang, J. Pu, L. Wang, Q. Xue, Frictional dependence of graphene and carbon nanotube in diamond-like carbon/ionic liquids hybrid films in vacuum, Carbon 80 (2014) 734–745.

[27] L. Zhang, J. Pu, L. Wang, Q. Xue, Synergistic effect of hybrid carbon nanotube-graphene oxide as nanoadditive enhancing the frictional properties of ionic liquids in High vacuum, ACS Appl. Mater. Interfaces 7 (2015) 8592–8600.
[28] X. Liu, J. Pu, L. Wang, Q. Xue, Novel DLC/ionic liquid/graphene nanocomposite coatings toward high-vacuum related space applications, J. Mater. Chem. A 1 (2013) 3797–3809.
[29] X. Chen, X. Yin, W. Qi, C. Zhang, J. Choi, S. Wu, R. Wang, J. Luo, Atomic-scale insights into the interfacial instability of superlubricity in hydrogenated amorphous carbon films, Sci. Adv. 6 (13) (2020) eaay1272, https://doi.org/10.1126/sciadv.aay1272.
[30] X. Chen, J. Li, Superlubricity of carbon nanostructures, Carbon 158 (2020) 1–23.
[31] Y. Wang, N. Yamada, J. Xu, J. Zhang, Q. Chen, Y. Ootani, Y. Higuchi, N. Ozawa, M. I.D.B. Bouchet, J.M. Martin, S. Mori, K. Adachi, M. Kubo, Triboemission of hydrocarbon molecules from diamond-like carbon friction interface induced atomic-scale wear, Sci. Adv. 5 (2019) eaax9301.
[32] X. Li, X. Xu, Y. Zhou, K.R. Lee, A. Wang, Insights into friction dependence of carbon nanoparticles as oil-based lubricant additive at amorphous carbon interface, Carbon 150 (2019) 465–474.
[33] A. Erdemir, G. Ramirez, O.L. Eryilmaz, B. Narayanan, Y. Liao, G. Kamath, S.K.R. S. Sankaranarayanan, Carbon-based tribofilms from lubricating oils, Nature 536 (2016) 67–71.
[34] H. Okubo, C. Tadokoro, S. Sasaki, Tribological properties of a tetrahedral amorphous carbon (ta-C) film under boundary lubrication in the presence of organic friction modifiers and zinc dialkyldithiophosphate (ZDDP), Wear 332–333 (2015) 1293–1302.
[35] T. Kuwahara, P.A. Romero, S. Makowski, V. Weihnacht, G. Moras, M. Moseler, Mechano-chemical decomposition of organic friction modifiers with multiple reactive centres induces superlubricity of ta-C, Nat. Commun. 10 (2019) 151.
[36] S. Plimpton, Fast parallel algorithms for short-range molecular dynamics, J. Comp. Phys. 117 (1995) 1–19.
[37] X. Li, P. Ke, H. Zheng, A. Wang, Structure properties and growth evolution of diamond-like carbon films with different incident energies: a molecular dynamics study, Appl. Surf. Sci. 273 (2013) 670–675.
[38] X. Li, A. Wang, K.R. Lee, Tribo-induced structural transformation and lubricant dissociation at amorphous carbon/alpha olefin interface, Adv. Theory Simul. 2 (2019) 1800157.
[39] H.J.C. Berendsen, J.P.M. Postma, W.F. van Gunsteren, A. DiNola, J.R. Haak, Molecular dynamics with coupling to an external bath, J. Chem. Phys. 81 (1984) 3684–3690.
[40] X. Li, A. Wang, K.R. Lee, Insights on low-friction mechanism of amorphous carbon films from reactive molecular dynamics study, Tribol. Int. 131 (2019) 567–578.
[41] X. Li, A. Wang, K.R. Lee, Mechanism of contact pressure-induced friction at the amorphous carbon/alpha olefin interface, npj Comput. Mater. 4 (2018) 53.
[42] G. Zilibotti, S. Corni, M.C. Righi, Load-induced confinement activates diamond lubrication by water, Phys. Rev. Lett. 111 (2013), 146101.
[43] T.B. Ma, L.F. Wang, Y.Z. Hu, X. Li, H. Wang, A shear localization mechanism for lubricity of amorphous carbon materials, Sci. Rep. 4 (2015) 3662.
[44] F. Tavazza, T.P. Senftle, C. Zou, C.A. Becker, A.C.T. Van Duin, Molecular dynamics investigation of the effects of tip-substrate interactions during nanoindentation, J. Phys. Chem. C 119 (2015) 13580–13589.
[45] X. Li, D. Zhang, X. Xu, K.R. Lee, Tailoring the nanostructure of graphene as an oil-based additive toward synergistic lubrication with an amorphous carbon film, ACS Appl. Mater. Interfaces 12 (2020) 43320–43330.
[46] A. Stukowski, Visualization and analysis of atomistic simulation data with OVITO–the Open Visualization Tool, Modelling Simul. Mater. Sci. Eng. 18 (2010), 015012.
[47] X. Li, A. Wang, K.R. Lee, Atomistic understanding on friction behavior of amorphous carbon films induced by surface hydrogenated modification, Tribol. Int. 136 (2019) 446–454.
[48] K.C. Mutyala, Y.A. Wu, A. Erdemir, A.V. Sumant, Graphene-MoS_2 ensembles to reduce friction and wear in DLC-Steel contacts, Carbon 146 (2019) 524–527.
[49] T.B. Ma, Y.Z. Hu, H. Wang, Molecular dynamics simulation of shear-induced graphitization of amorphous carbon films, Carbon 47 (2009) 1953–1957.
[50] S. Bai, H. Murabayashi, Y. Kobayashi, Y. Higuchi, N. Ozawa, K. Adachi, J. M. Martin, M. Kubo, Tight-binding quantum chemical molecular dynamics simulations of the low friction mechanism of fluorine-terminated diamond-like carbon films, RSC Adv. 4 (2014) 33739–33748.
[51] X. Li, A. Wang, K.R. Lee, Role of unsaturated hydrocarbon lubricant on the friction behavior of amorphous carbon films from reactive molecular dynamics study, Comput. Mater. Sci. 161 (2019) 1–9.
[52] B.R. Höhn, K. Michaelis, Influence of oil temperature on gear failures, Tribo. Int. 37 (2004) 103–109.
[53] X. Liu, R. Yamaguchi, N. Umehara, M. Murashima, T. Tokoroyama, Effect of oil temperature and counterpart material on the wear mechanism of ta-CNx coating under base oil lubrication, Wear 390–391 (2017) 312–321.
[54] T. Yamaguchi, J. Ando, T. Tsuda, N. Takahashi, M. Tohyama, A. Murase, T. Ohmori, K. Hokkirigawa, Sliding velocity dependency of the friction coefficient of Si-containing diamond-like carbon film under oil lubricated condition, Tribo. Int. 44 (2011) 1296–1303.
[55] Y. Guo, P. Guo, L. Sun, X. Li, P. Ke, Q. Li, A. Wang, Tribological properties of Ti-doped diamond-like carbon coatings under dry and PAO oil lubrication, Surf. Interface Anal. 51 (2019) 361–370.
[56] M. Kobayashi, M. Kaido, A. Suzuki, A. Takahara, Tribological properties of cross-linked oleophilic polymer brushed on diamond-like carbon films, Polymer 89 (2016) 128–134.
[57] I. Velkavrh, M. Kalin, J. Vizintin, The influence of viscosity on the friction in lubricated DLC contacts at various sliding velocities, Tribo. Int. 42 (2009) 1752–1757.
[58] X. Li, A. Wang, K.R. Lee, Transformation of amorphous carbon to graphene on low-index Ni surfaces during rapid thermal processing: a reactive molecular dynamics study, Phys. Chem. Chem. Phys. 21 (2019) 2271–2275.